SWASH ZONE DYNAMICS ON AN INTERMEDIATE ENERGY REFLECTIVE BEACH

Jose C. Pintado-Patiño[1], Alec Torres-Freyermuth[1], Jack A. Puleo[2] and Gerben Ruessink [3]

Abstract

We investigate swash dynamics on an intermediate-energy reflective beach by means of a nonlinear wave transformation model which solves the Reynolds-Averaged Navier-Stokes equations with a VOF-tracking scheme and a κ - ε turbulence closure. A reference frame oriented parallel to bed is implemented in order to resolve boundary layer dynamics in the swash zone. Offshore pressure and velocity measurements during the BARDEX II experiment are employed for the model forcing and validation in the inner surf zone. Moreover, highly-resolved velocity measurements within the swash zone are employed for the model validation inside the swash zone. The model results indicate its capability to simulate complex flow conditions induced by nonlinear (irregular) wave transformation seaward and within the swash zone. Subsequently, the numerical model is applied to study bed shear stresses and wave run-up. The study of the spatial/temporal evolution of turbulence kinetic energy and bed shear stresses in the swash zone is part of the ongoing research.

Key words: Swash zone, nearshore dynamics, bottom boundary, shear stresses, numerical simulation

1. Introduction

The intermittent incursion/excursion of (shallow) depth varying and turbulent water flows define the hydro-dynamical forcing acting on the foreshore (Puleo et al., 2007). Thus, near bed processes inside the swash zone are critical for sediment mobility estimation and rates of sediment exchange as an integral part of the nearshore region. Even though understanding of swash zone dynamics has improved, a complete description of the processes at different spatial-time scales remains un-resolved. In general, laboratory studies (e.g., Petti and Longo, 2001; Cowen et al., 2003; Barnes et al., 2009; O'Donogue et al., 2010) have yielded advancements but may be limited to the physical and wave conditions used. Measurements in natural settings are more difficult due to shallow water depths and changing seabed levels (Aagaard and Hughes, 2006; Blenkinsopp et al., 2011). Nonetheless, recent advancement in small Acoustic Doppler current profilers allows the collection of velocity profiles at high spatial and temporal resolution (Puleo et al., 2012) for most part of the swash flow duration. These high-resolution data sets provide new information for testing numerical model capability within the swash zone. In turn, a validated numerical approach can provide further information where measurements are lacking in an effort to better quantify boundary layer dynamics and turbulent properties in this complex region.

Puleo et al. (2012) provided field evidence of the vertical profile of the horizontal velocity within the boundary layer of two natural beaches under mild wave conditions. The high-resolution measurements were sampled at a frequency up to 100 Hz with a vertical resolution of 0.001 m near the bed. The suitability of the logarithmic model fit with respect to the measured velocity profiles was successfully tested ($r^2 > 0.9$) until a cut off height of 0.02 m above the bed. The latter was found for most of the swash cycles when the boundary layer is clearly defined, as opposed to times when velocities are low (i.e., near flow reversal). The velocity measurements were further employed to estimate bed shear stress using the quadratic drag law. Reported maximum shear stress magnitudes of 6.45 Nm^{-2} were in agreement with

[1] Laboratorio de Ingeniería y Procesos Costeros, Instituto de Ingeniería, Universidad Nacional Autónoma de México, S isal, Yucatán México. JPintadoP@iingen.unam.mx, ATorresF@ii.unam.mx

[2]Ocean Engineering Laboratory, Center for Applied Coastal Research, Department of Civil and Environmental Engineering, University of Delaware, Newark, DE USA. jpuleo@udel.edu

[3] Faculty of Geosciences, Utrecht University, Utrecht, 3508 TC, The Netherlands. B.G.Ruessink@uu.nl

laboratory (e.g., O'Donogue et al., 2010) and direct field measurements (e.g., Conley and Griffin, 2004) under similar flow conditions. The latter provides confidence on the use of the logarithmic model as a proxy to velocity profile estimation, consistent with Raubenheimer et al. (2004) and Masselink et al. (2005). Furthermore, the dependence on the number of points within the velocity profile used in the quadratic law was highlighted by equating friction velocities, friction factors, and corresponding bed shear stresses.

On the other hand, numerical models have been successfully employed for the study of swash hydrodynamics. The implementation of seaward/landward boundary conditions has been one of the major challenges in the modelling of this region (Brochini and Baldock, 2008). Boussinesq (Madsen et al., 1997; Baird et al., 1998; Kennedy et al., 2000; Sørensen, 2004) and nonlinear shallow water (NLSW) (e.g., Hughes and Baldock,2004; O'Donogue et al., 2010) equations are able to describe the depth-averaged flow conditions in this region. Nonetheless, boundary layer dynamics, which are key processes for sediment transport, can be only incorporated through the coupling with boundary layer models while employing these modelling approaches (e.g., Brigganti et al., 2011). Furthermore, most of these models do not provide turbulence information. More recently, Torres-Freyermuth et al. (2013) validated a numerical model solving the Reynolds-Averaged Navier-Stokes equations (RANS) by comparing results from simulations and the ensemble-average dam-break driven swash experimental data from O'Donoghue et al. (2010). Model-data comparison for run-up distance, near bed velocities, boundary layer thickness, bed shear stresses, and turbulent kinetic energy illustrated the model capability for the high-resolution modelling in this region. Thus, recent advances in both measuring techniques and numerical modelling have contributed to improve our understanding of swash zone dynamics.

Shared research initiatives have allowed more robust measuring techniques under both controlled and natural conditions. For instance, the large-scale Barrier Dynamics Experiment for a gravel (BARDEX) and a sand beach barrier (BARDEX II) aims to study those processes related to overwash, cross barrier swash/groundwater fluxes, and the role of groundwater table on beach stability (Williams *et al.*, 2012; Masselink et al., 2013). BARDEX II experiments have generated new data sets of cross-shore hydrodynamics, morphological development in the swash zone, and sediment exchange between the swash and surf zone (Masselink et al., 2013). Measurements from more than 200 deployed instruments at prototype conditions will allow significant contributions in a range of nearshore conditions, including swash zone dynamics.

The present work aims to validate a two-dimensional vertical (2DV) RANS-VOF numerical model for the study of swash flow under realistic (irregular waves) forcing conditions at a prototype scale. For the model validation, we employed high-resolution velocity data, obtained during the BARDEX II experiment, from the swash zone. The outline of this paper is as follows. A brief description of the experimental setup is provided in section 2. In section 3, a general description of the numerical model followed by the numerical implementation of the simulated cases and some acknowledged constraints in the current simulations. The model validation with laboratory data is presented in section 4. Finally, concluding remarks and ongoing work are appointed in section 5.

2. Experimental setup

The Barrier Dynamics Experiment (BARDEX II) funded under the Hydralab IV programme entailed the collaboration of almost 30 researchers from several research institutions (Masselink et al., 2013). The experiment was conducted in the Delta Flume (240 m-long, 5 m-wide, 7 m-deep) from 07/06/2012 until 04/07/2012. The initial overall experiment consisted of a 4.5-m high and 40-m wide sandy barrier with a concrete toe, followed by a β=0.143 ($\approx$1/7) sand slope, a flat section, and lagoon reservoir situated on the landward section (Figure 1). During the experiments some parameters such as the sediment size (D_{90} = 0.3 mm; D_{50} = 0.5 mm; D_{10} = 0.9 mm), porosity P (37–42%), and the hydraulic conductivity K of sediment (0.0005–0.001 mm s^{-1}) were kept constant. On the other hand, parameters such as sea water level, lagoon water level, beach morphology and the irregular wave characteristics (with H_s = 0.8 m, and Tp =4-12 s) were varied between tests. The data employed in this paper correspond to pressure and velocity measurements at different cross-shore locations including the sub-aerial beach profile. Figure 1 shows the experimental setup and the sensors locations employed in this work.

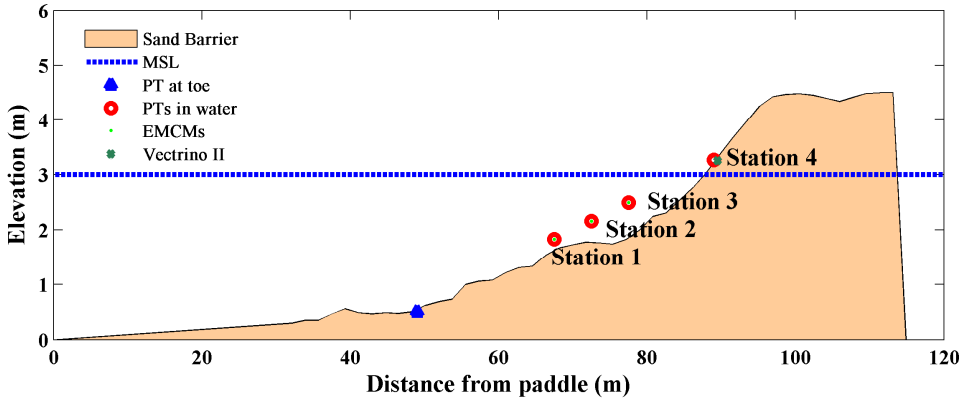

Figure 1. BARDEX II experimental setup and computation domain. The reference frame in the numerical model is oriented bed parallel and bed orthogonal to bed. Numerical results from a coarse mesh resolution *(black dash square)* were employed for the forcing of a fine mesh (*red dashed square)* in order to resolve boundary layer processes within the swash zone.

3. Numerical model

3.1 *Model formulation*

The depth- and phase-resolving Cornell Breaking Wave and Structures (COBRAS) numerical model, developed by Lin and Liu (1998), is employed in this work. The numerical model is based on a 2D fluid dynamics model developed at Los Alamos National Laboratory known as RIPPLE (Kothe et al., 1991), which solves the 2D RANS equations:

$$\frac{\partial < u_i >}{\partial x_i} = 0 \tag{1}$$

$$\frac{\partial < u_i >}{\partial t} + < u_j > \frac{\partial < u_i >}{\partial x_j} = -\frac{1}{\rho}\frac{\partial < p >}{\partial x_i} + g_i + \frac{1}{\rho}\frac{\partial < \tau_{ij} >}{\partial x_j} - \frac{\partial < u_i' u_j' >}{\partial x_i} \tag{2}$$

where angle brackets denote Reynolds averaged quantities, t is time, x_i the bed parallel and orthogonal coordinate ($i=1,2$ correspondingly), g_i is the ith gravitational component, u_i is the fluid velocity in direction x_i, ρ is the fluid density, p refers to pressure, τ_{ij} is the shear stress of the mean flow, and $\rho\langle u_i' u_j' \rangle$ denote the Reynolds stresses which are approximated with a κ - ε turbulence closure scheme.

The scheme of turbulent kinetic energy production and dissipation rate (κ - ε) equations are derived from the Navier Stokes equations and by replacing higher order correlation coefficients of turbulence fluctuations with closure conditions. Empirical coefficients determined for stationary flow are used during ε estimation. A nonlinear algebraic Reynolds stress model relates the Reynolds stress tensor and the strain rate of mean flow (Lin and Liu, 1998; Rodi, 1993). Finite difference with two step projection is used for solving the RANS equations, and the volume of fluid (VOF) method (Hirt and Nichols, 1990) is used for the free surface, identified by integrating the VOF value over depth at the centre of each cell. Further in depth formulation and description of the model is given in Lin and Liu (1998) and Losada et al. (2008). This numerical model has been successfully validated for the study of wave-structure interaction (e.g., Hsu et al., 2002; Lara et al., 2006a; Losada et al., 2008), surf zone hydrodynamics (e.g. Lin and Liu, 1998a; Lin and Liu, 1998b; Lara et al., 2006b; Torres-Freyermuth et al., 2007; Torres-Freyermuth et al., 2010; Pedrozo-Acuña et al., 2010), swash zone hydrodynamics (e.g., Zhang and Liu, 2008; Torres-Freyermuth et al., 2013), and wave-mud interaction (Hsu et al., 2013).

3.2 *Numerical Setup*

Despite increases in computational power and more robustness in numerical approaches, constraints on the numerical modelling of wave transformation using a high resolution simulation scheme still exist. Therefore, grid characteristics must be carefully prioritized in order to improve model performance and resolve the physics of the process of interest.

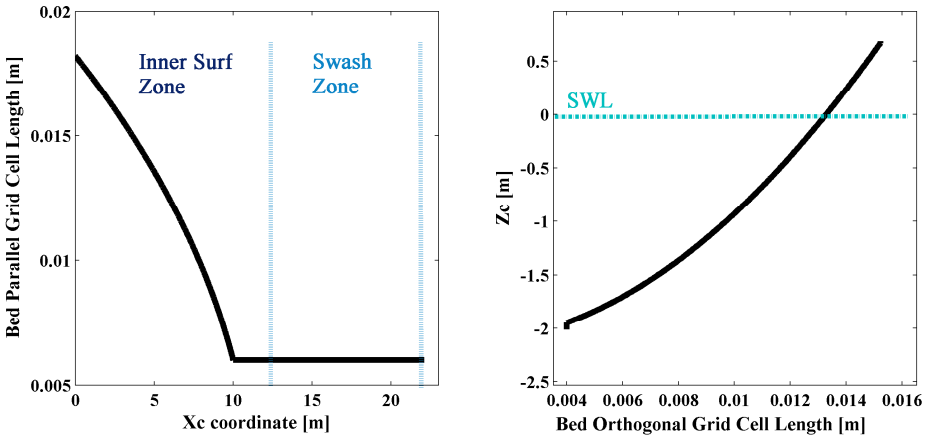

Figure 2. Horizontal (left) and vertical (right) non-uniform grid variation within the computational domain.

A bed parallel (*Xc*) and bed orthogonal (*Zc*) coordinate system is adopted in order to resolve the swash zone hydrodynamics (e.g., Puleo et al., 2007; Zhang and Liu, 2008; Torres-Freyermuth et al., 2013). This allows a higher resolution near the bed and avoids spurious pressure owing to the partial cells treatment (Zhang and Liu, 2008). The numerical model is forced with free-surface elevation derived from the measured pressure at the toe of the barrier slope (x=49 m) employing linear wave theory. Separation of incident and reflected wave components is not considered in these initial simulations and hence an over prediction of the incident wave energy can be expected. A coarse grid domain (Δxc_{min}=0.01 m and Δzc_{min}=0.01 m) is first employed in order to simulate wave transformation from the toe of the sand barrier (x=49 m) until the shore using a non-uniform grid system grid consisting of 2602x282 cells. Subsequently, free-surface elevation and velocity profiles at the inner surf zone are further employed as the forcing condition of another simulation using a higher grid resolution (Δxc_{min}=0.006 m and Δzc_{min}=0.004 m; 2842x290 cells). The latter allows us to achieve a higher spatial resolution at the swash zone (*see* Fig. 2). It is worth mentioning that the use of a coarser mesh domain and finer nested mesh is effective in decreasing computational time while allowing a higher mesh resolution at the zone of interest. The velocity information at the forcing boundary of the finer mesh domain contains incident and reflected wave information. A summary of the simulated tests/characteristics is shown in Table1.

Table 1. Simulated cases. The significant wave (Hs), peak period (Tp), sea water level (SWL), time of simulation (Tsim) and the computational time (Texe) are presented for the simulated cases. Simulations were performed using an Intel Xeon 2.53 GHz (6GB RAM) computer.

Test	Grid Domain	H_s [m]	T_p [s]	SWL [m]	T_{sim} [s]	T_{exe} [h]
B2c02	Coarse	0.8	8	2.5	512	≈ 6
B2c06	Coarse	0.8	8	2.5	512	≈ 6
B1c05a	Coarse	0.8	8	3.0	512	≈ 6
B1c05b	Fine	0.8	8	3.0	120	≈ 143

4. Results

4.1 *Wave Forcing*

The numerical model is forced with the free-surface elevation and velocity profiles derived using linear wave theory. As previously mentioned, separation between incident and reflected wave conditions is not considered and hence the measured signal at the forcing location is considered to be onshore directed. Figure 3 shows the measured wave spectra and time series at the forcing location (x=49 m). We test the wave generation performance by comparing the measured and simulated free-surface elevation (Figure 3b). Differences between measured and simulated time series increased with time. The latter highlights the importance of separation of incident and reflected waves for the model forcing that will be conducted in future simulations. However, when considering the total measured signal for the wave forcing, the simulation presents a satisfactory agreement with the data during the first 150 s (Figure 3b). Another source of differences can be ascribed to the morphological changes in the laboratory that are not accounted in the numerical model. For the simulated wave conditions, the Iribarren number ($Ir \approx 0.25$) was typical for dissipative to intermediate conditions, with no significant contribution of long period oscillation waves for the time considered as shown below.

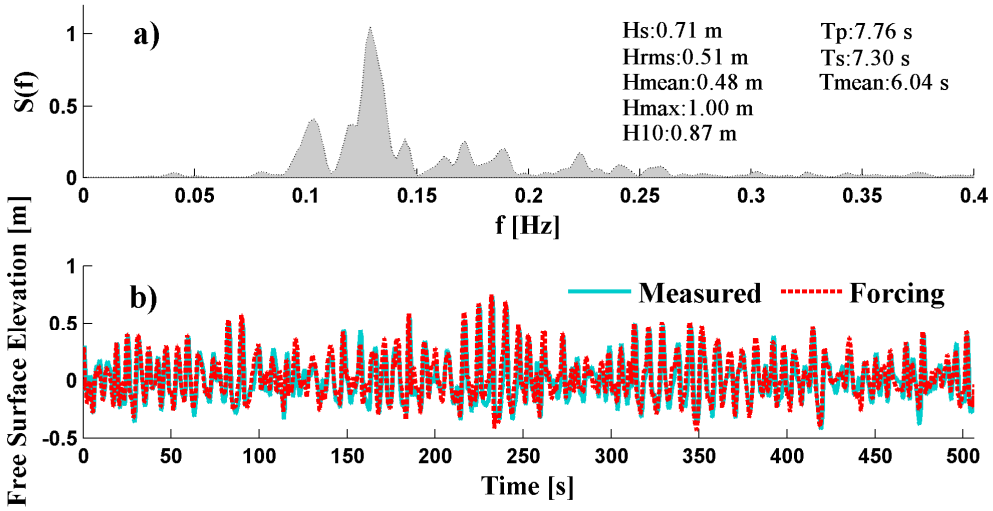

Figure 3. *(a)* Spectral characteristics employed as the forcing wave signal.
(b) Measured and simulated time series at the forcing boundary.

4.2 *Model-Data Comparisons in the inner surf zone.*

The numerical model is first validated with pressure and velocity time series measured by the pressure transducer and electromagnetic current meter (PT-ECM) co-located at each station of Figure1. Therefore, in this section we present model-data comparison at x=67.5 (Station 1), 72.5 (Station 2), and 77.5 (Station 3) m. The numerical model resolves the vertical structure of the flow and hence the model-data comparisons are conducted at the exact horizontal/vertical location. In general a good agreement for both dynamic pressure and horizontal velocity is observed at all the stations. At Station 1 (Figure 4), the numerical model predicts the magnitude and phase of the wave induced pressure and velocity. Consistent with the simulated time series at the forcing boundary, differences increase between measured and predicted results with increasing computational time. Similarly, at Station 2 (x=*72.5 m* in Figure 1) mean relative differences of less than 5% are obtained for pressure and horizontal velocities. Furthermore, pressure and velocity ranges of 1.649- 1.048 kg/cm^2 and 1.574 m/s- -0.774 m/s (see Figure 5) are consistent with the measured values

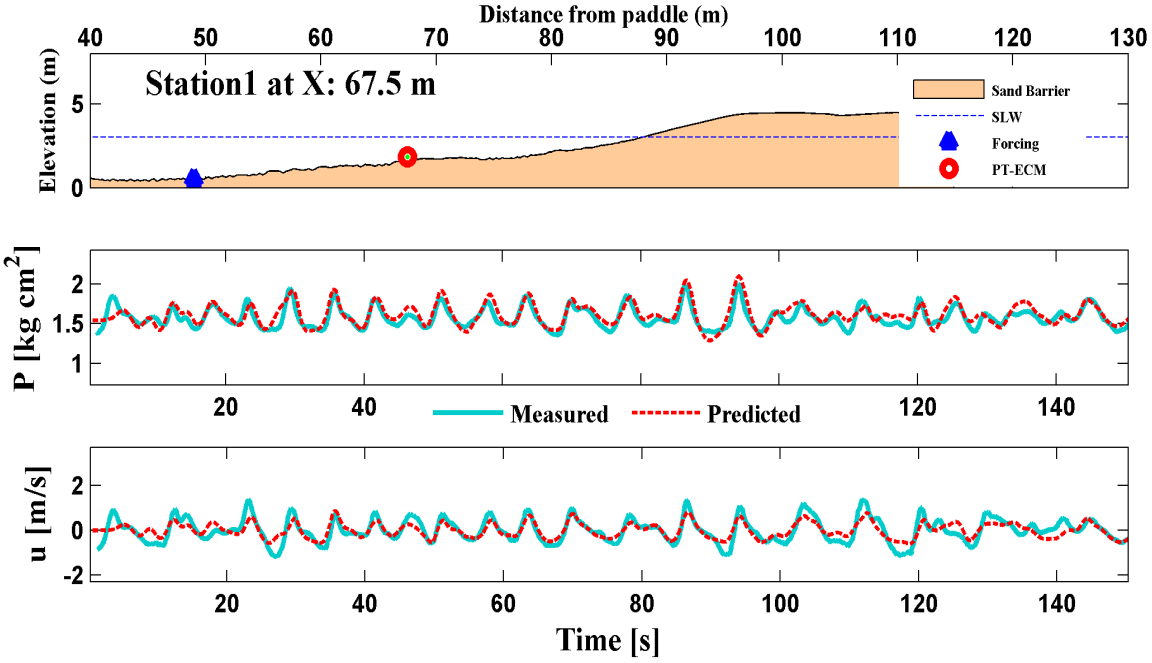

Figure 4. Measured (*light blue*) and predicted (*dashed-red*) bottom pressure and velocity time series at Station 1.

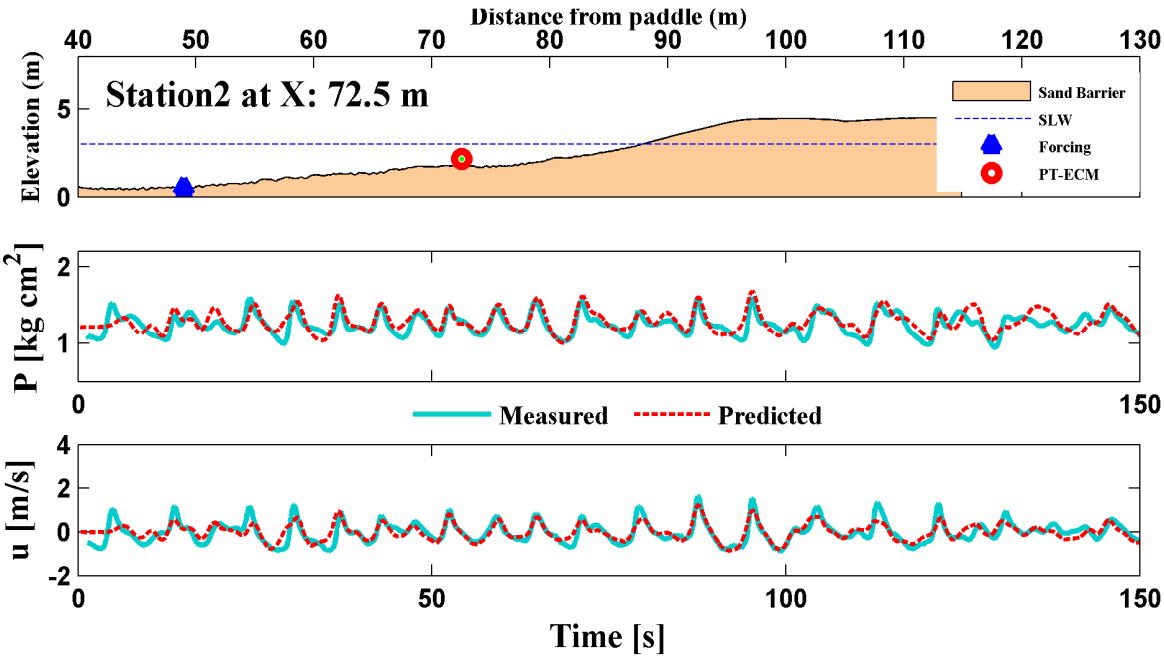

Figure 5. Measured (*in light blue*) and predicted (*in dashed red*) bottom pressure and velocity time series at Station 2.

.

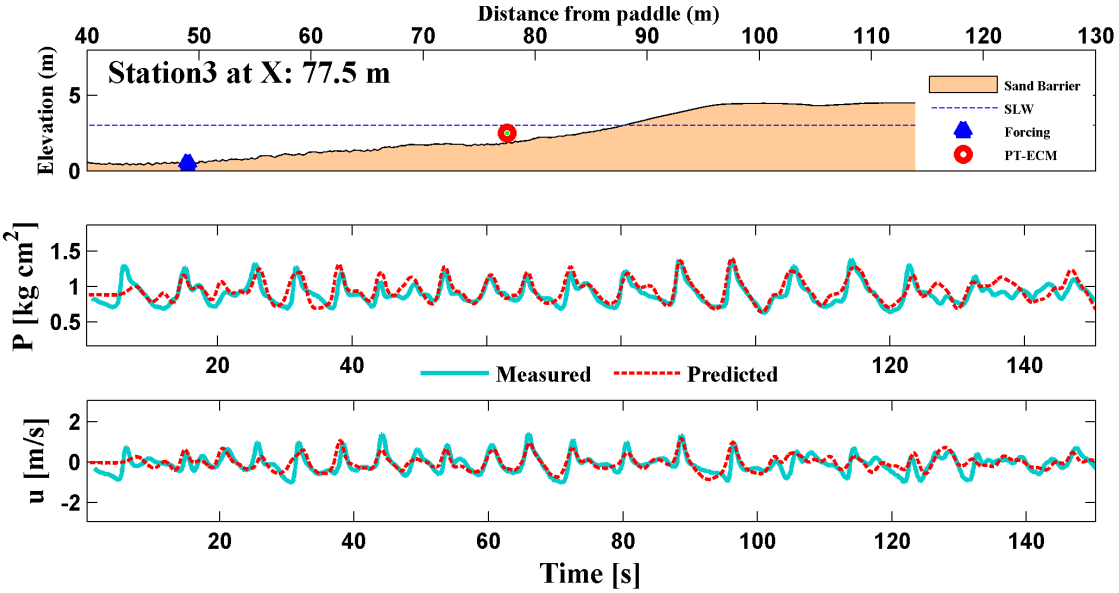

Figure 6. Measured (*light-blue*) and predicted (*dashed-red*) mid water pressure and velocity time series at Station 3.

Finally, at the measurements Station 3 (x= *77.5 m* in Figure 1) the instruments are located at mid water elevation between the still water level and the seabed. Measured and predicted pressure/velocity time series at this location are shown in Figure 6. Predicted magnitudes are near those magnitudes from measurements, ranging between 1.186 and -0.706 m/s. Maximum values of 1.374 and 0.6755 kg/cm^2 where found for measured and predicted (correspondingly) mid water pressure, with a 5.84 % mean relative error between signals for this case. Moreover, the skewness and asymmetry is well resolved.

Table 2. Mean relative differences of wave statistics between measurements and predictions for stations 1, 2 and 3.

H_{rms} [%]	T_p [%]	γ_b [%]	m_0 [%]
3.58	16.41	6.12	6.57

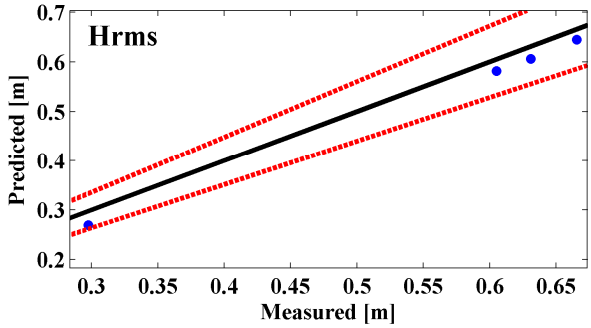

Figure 7. Measured versus predicted root mean square wave height for all stations.
Solid line: perfect agreement; *dashed red line*: ± 10% confidence interval bounds.

Measured and predicted breaking index parameter ($\gamma_b = H_{rms} / h$) estimated at Stations 1 (x=67.5 m) and 2 (x=72.5 m) are in good agreement with field observations (e.g., Raubenheimer, 2002) with values of 0.40/0.37 and 0.48/0.45 for measured/predicted, respectively. At Station 3 (x=77.5 m), values of γ_b = 0.74 and γ_b = 0.68 for measured/predicted estimates were found. Moreover, the average accounting for the relative differences found at each station located in the surf zone (Stations 1-3) results in a mean relative difference of 6.12% for the case of γ_b. Similarly, acceptable mean relative errors for the root mean square wave height (H_{rms}), peak wave period (T_p), and variance (m_0) are obtained (Table 2).

4.3 *Model-Data Comparisons in the swash zone.*

The modeling of swash zone hydrodynamics is based on the nesting of a higher resolution mesh using the coarse mesh results. Velocity information in the swash zone (x= *89 m*) was acquired with a Pulse Coherent Acoustic Doppler Profiler (PC-ADCP) Vectrino II capable of resolving boundary layer profiles (e.g., Puleo et al. 2012). The horizontal velocity time series at this location were measured at 100 Hz sample frequency over the range of 0.002 -0.032 m at 0.001 m bin spacing. The measurements are compared with the predicted velocities from the model output at 0.010 m vertical distance above the bed. At this location (x= *89 m*), difference between the dynamic pressure time series resulted in 12.09%, denoting that the model is able at least to predict most of the important wave events at the swash zone. The time series of predicted velocity oscillates from -2.702 m/s to 3.39 m/s with the arrival of incoming bore flows during the up-rush, and smoother transitions for the case of the back-wash as depicted in Figure 8. The gaps in the PC-ADCP indicate intermittency in the swash measurements when the water depth falls below the measuring region of the sensor and also indicates the difficulty in capturing velocities in aerated, shallow swash flows (Figure 9).

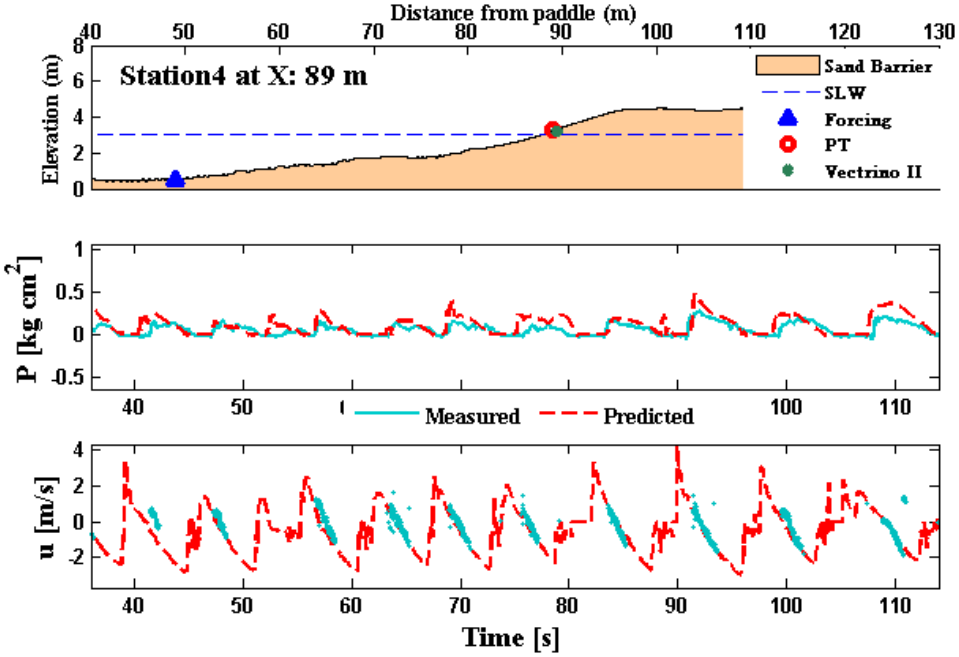

Figure 8. Dynamic pressure and velocity time series at station 4 (measured: *light blue*; predicted: *dashed red*).

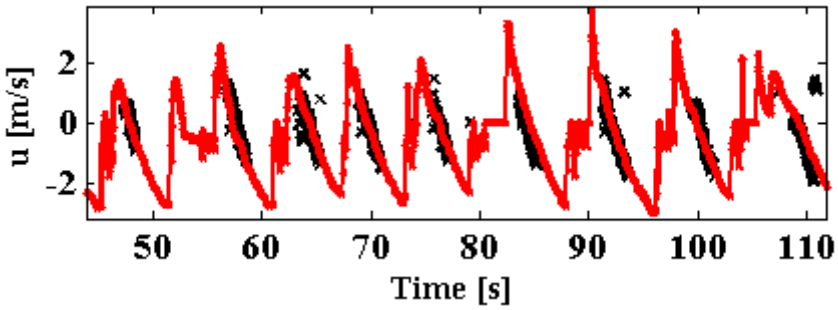

Figure 9. Zoom of measurements and predicted horizontal velocity time series at 0.01 m above bed.

A range of 2.888 to -2.920 m/s for measured and of 3.396 to -2.917 m/s for predicted horizontal velocities within 0.01 m from bed are found. Data from the Vectrinos II measurements has been removed using a

correlation cutoff of 60%. Therefore a comparison between signals for the total time length is lacking. The measurements are less reliable during the peak uprush/back wash. However, a relative percentage error of 17.67% is found for the times where reliable data exists. Vectrino II data will be further quality-controlled in future model-data comparisons.

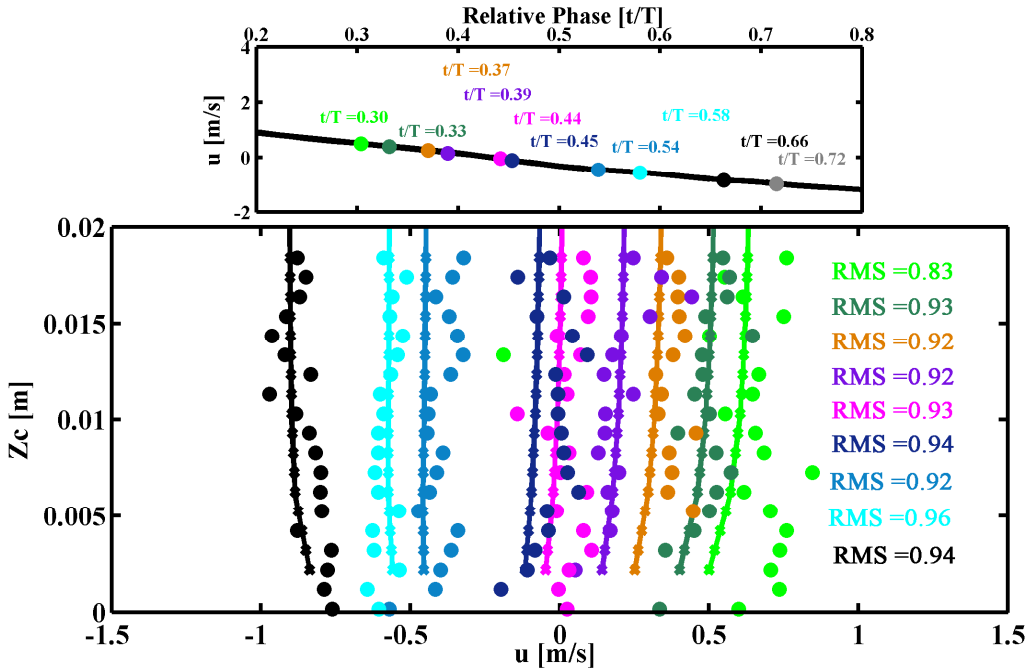

Figure 10. Measured (*colored filled circles*) and predicted (*colored crossed lines*) horizontal velocity profile for a swash event from bed until 0.02m above bed and corresponding root mean square error (RMS) obtained values.

The horizontal velocities at different vertical positions above the bed and for different relative phases after normalization of swash events are also employed for model testing. Estimations of the root mean square errors (RMS) between measured and predicted horizontal velocities denote the model capability to resolve the velocity profile (Figure 10).

4.4 *Model application*

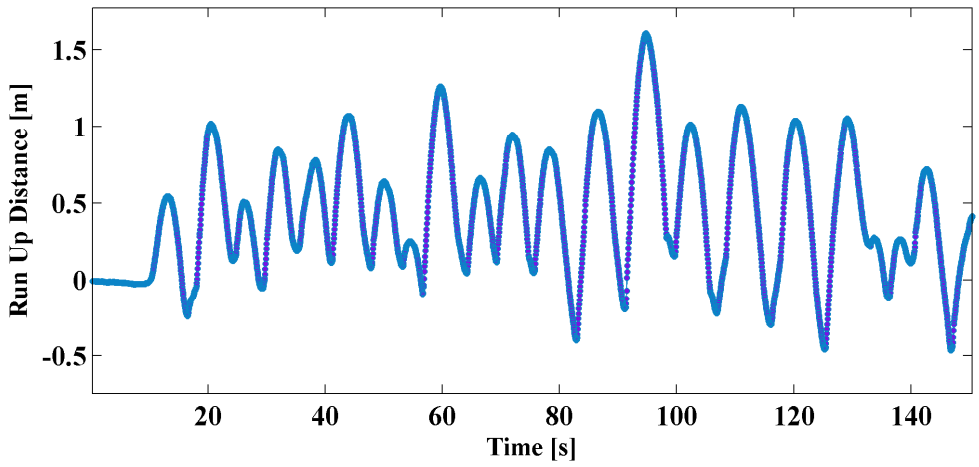

Figure 11. Predicted time series of run up distance evolution from still water (x=87.5 m).

The previous results have motivated the model application to investigate swash zone hydrodynamics under irregular forcing at prototype scale. For instance, the evolution of the run-up in the beach face can be extracted by tracking the wet-dry interface in the numerical model (Figure 11). It is shown a maximum excursion of 1.6 m from the intersection of the still water level with the sand barrier slope for the simulated period. These results will be validated in the future with video images at this region.
On the other hand, the bed shear stresses can be also extracted directly from the numerical model (e.g., Torres-Freyermuth et al. 2013). The varying water depth at a location in the mid swash zone (x=91.5 m away from the paddle and 52.79% of immersed time) has been extracted in order to perform event by event analysis. Swash events longer than 4.2 s are normalized by their total duration and maximum height in an effort to obtain similarity between events as depicted in figure 12a for 50s of simulation time.

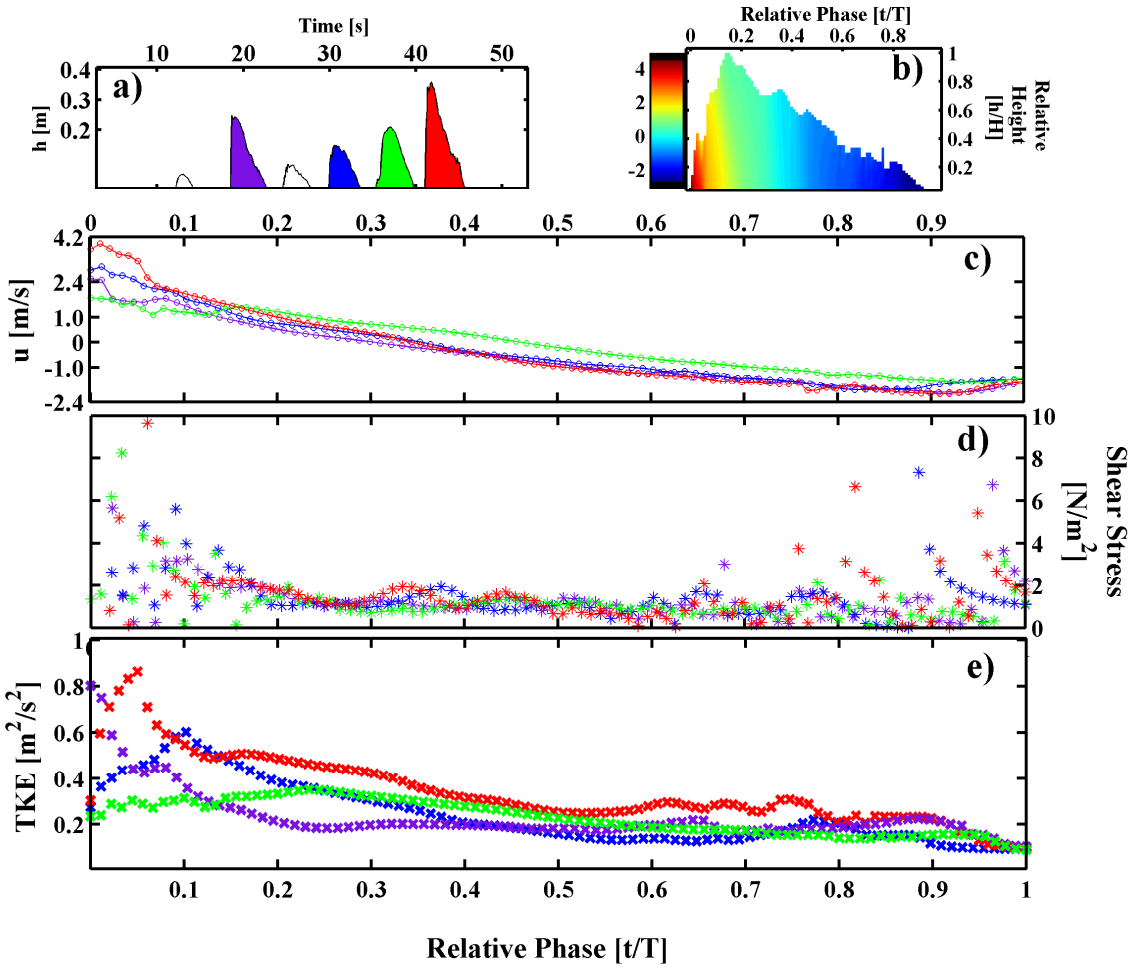

Figure 12. (a) Varying water depth evolution at x= 91.5 m. (b) Time and height normalization of swash event depicted as red in a). The color bar indicates cross-shore velocity [m/s] at 0.002m above the bed. (c) Horizontal velocities; (d) Bed shear stresses and (e) turbulent kinetic energy of predicted swash events.

At this mid swash location, the up-rush horizontal velocity at Zc = 0.002m results higher than that of the backwash for all swash cycles considered (-2.02 m/s to 3.92 m/s for the most energetic event depicted as red in Figure 12a). The later results also true from peak shear stresses and turbulent kinetic energy, consistent with previous results. Estimated peak shear stresses are found to be slightly higher ($\tau_{up\text{-}rush}$ = 13.56 N/m^2 and $\tau_{back\text{-}wash}$ = 6.6 N/m^2 for the same event) during the onshore-directed flow as similar to the direct estimates of Conley and Griffin (2004).

5. Conclusions

A numerical model based on the RANS equation is employed in order to investigate swash zone dynamics. Numerical modeling of swash flow induced by irregular wave transformation at a near prototype scale is a challenging task for the different spatial-temporal scales involved. First, the numerical model is validated with pressure and velocity time series at different cross-shore locations within the inner surf zone. Subsequently, model predictions at the inner surf zone are further employed for the forcing of a higher resolution mesh covering the swash zone. We employed high-resolution velocity information for a preliminary model validation of the numerical results in the swash zone. Examples of the model application for the study of wave run-up and bed-shear stresses are presented. Future work will consider the study of cross-shore turbulence distribution and its time evolution during both phases of the swash motion.

Acknowledgements
José C. Pintado-Patiño acknowledges the financial support provided by the Mexican National Council of Science and Technology (CONACyT) for his PhD studies under the scholarship number 490080. Financial support was provided by the National Council of Science and Technology of Mexico (CB-167692) and Universidad Nacional Autónoma de México (Instituto de Ingenieria Proyecto Interno A2 and DGAPA UNAM PAPIIT IB102012-2). This material is based upon work supported by the National Science Foundation under Grant No. OCE-0845004. The Bardex II experiment was supported by the European Community's 7th Framework Programme through the grant to the budget of the Integrating Activity HYDRALAB IV, contract no. 261520. Additional support for this work was provided by the University of Delaware and the US/UK Fullbright Commission.

6. References

Aagaard, T., and Hughes, M. G., 2006. Sediment suspension and turbulence in the swash zone of dissipative beaches. *Marine Geology*, 228(1-4): 117-135.

Baird, A.J., Mason, T., Horn, D.P., 1998. Validation of a Boussinesq model of beach ground water behaviour. *Marine Geology.* 148: 55– 69.

Barnes, M. P., O'Donoghue, T., Alsina, M. J., and Baldock, T. E.., 2009. Direct bed shear stress measurements in bore-driven swash. *Coastal Engineering*, 56 (8): 853- 867.

Blenkinsopp, C. E., I. L. Turner, G. Masselink, and P. E. Russell., 2011. Swash zone sediment fluxes field observations, *Coast. Eng. Japan*, 58, 28-44.

Briganti,R.,N.Dodd,D.Pokrajac, andT.O'Donoghue., 2011. Nonlinear shallow water modeling of bore driven swash: Description of the bottom boundary layer. Coastal Engineering, 58(6), 463–477, doi:DOI: 10.1016/j.coastaleng.2011.01.004.

Brocchini, M., & Baldock, T. E., 2008. Recent advances in modeling swash zone dynamics: influence of surf-swash interaction on nearshore hydrodynamics and morphodynamics. *Reviews of Geophysics*, 46 (RG3003).

Conley, D. C., & J. G. Griffin., 2004. Direct measurements of bed stress under swash in the field. Journal of Geophysical Research, 109(3), C03050, 1-12.

Cowen, E. A., I. M. Sou, P. L.-F. Liu, and B. Raubenheimer., 2003. Particle image velocimetry measurements within laboratory-generated swash zone. *Journal of Engineering Mechanics*, 129: 1119-1129.

Hirt, C. W., and B. D. Nichols (1990), Volume of fluid (VOF) method for dynamics of free boundaries. *J. Comput. Phys.*, 39: 201–225.

Hughes, M. G., and T. E. Baldock (2004), Eulerian flow velocities in the swash zone: Field data and model predictions. *Journal of Geophysiscal Research,Oceans*, 109(8), C08009, 1–11.

Hsu, W. Y., H. H. Hwung, T. J. Hsu, A. Torres-Freyermuth, and R. Y. Yang., 2013. An experimental and numerical investigation on wave-mud interactions. *Journal of Geophysical Research*, *Oceans*, 118., doi:10.1002/jgrc.

Kennedy, A.B., Chen, Q., Kirby, J.T. & Dalrymple, R.A. , 2000. Boussinesq modeling of wave transformation, breaking, and run up. I: 1D. *Journal of Waterway, Port, Coastal and Ocean Engineering*, 126-1: 39- 47.

Kothe, D. B., R. C. Mjolness, and M. D. Torrey (1991), RIPPLE: A computer program for incompressible flows with free surface. *Techinal Report, Rep*. 96-5., Los Alamos National Laboratory.

Lara, J.L., Garcia, N., Losada, I.J., 2006a. RANSmodelling applied to random wave interaction with submerged permeable structures. *Coastal Engineering*, 53, 395–417.

Lara, J.L., Losada, I.J., Liu, P.L.F., 2006b. Breaking waves over a mild gravel slope: experimental and numerical

analysis. *Journal of Geophysical Resesarch*, 111 (C11019)., doi:10.1029/2005JC003374.

Lin, P., and Liu, P. L. –F., 1998a. A numerical study on breaking waves in the surf zone. *Journal of Fluid Mechanics*, 359: 239-264.

Lin, P., and Liu, P. L., 1998b. Turbulence transport, vorticity dynamics, and solute mixing under plunging breaking waves in surf zone. *Journal of Geophysical Research*, 103(C8), 15,677-15,694.

Losada, I. J., J. L. Lara, R. Guanche, & J. M. González-Ondina., 2008. Numerical analysis of wave overtopping of high mound breakwaters. *Coastal Eng*., 55, 47–62.

Madsen,P.A.,Sørensen,O.R.,Schäffer,H.A.,1997. Surf zone dynamics simulated by a Boussinesq type model. PartII. Surf beat and swash oscillations for wave groups and irregular waves. *CoastalEngineering*, 32: 289–319.

Masselink, G., Evans, D., Hughes, M.G., & Russell, P., 2005. Suspended sediment transport in the swash zone of a dissipative beach. *Marine Geology*, 216: 169–189.

Masselink, G, Turner, I.L., Conley, D.C., Ruessink, B.G., Matias, A., Thompson, C., Castelle, B. and Wolters, G., 2013. BARDEX II: Bringing the beach to the laboratory – again! **In:** Conley, D.C., Masselink, G., Russell, P.E. and O'Hare, T.J. (eds.), Proceedings 12th International Coastal Symposium, *Journal of Coastal Research*, Special Issue, No. 65.

Miles, J., But, T., and P. Russell., 2006. Swash zone sediment dynamics: A comparison of a dissipative and an intermediate beach. *Marine Geology*, 231: 181-200.

O'Donoghue, T., D. Pokrajac, & L. Hondebrink., 2010. Laboratory and numerical study of dambreak-generated swash on impermeable slopes. *Coastal Engineering*, 57 (5): 513-530.

Pedrozo-Acuna, A., A. Torres-Freyermuth, Q. Zou, T.-J. Hsu, and D. E. Reeve., 2010. Diagnostic investigation of impulsive pressures induced by plunging breakers impinging on gravel beaches. *Coastal Engineering*, 57(3), 252–266., doi: 10.1016/j.coastaleng.2009.09.010.

Petti, M., and Longo, S., 2001. Turbulence experiments in the swash zone. *Coastal Engineering,* 43 (1), 1–24.

Puleo, J. A., and T. Butt., 2006. The 1st international workshop on swash-zone processes, *Continental Shelf Research*, 26: 556-560.

Puleo, J. A., A. Farhadzadeh., & N. Kobayashi., 2007. Numerical simulation of swash zone fluid accelerations. Journal of Geophysical Research, 112, C07007., doi:10.1029/2006JC004084.

Puleo, J. A., Lanckriet, T., and Wang, P., 2012[a]. Near bed cross-shore velocity profiles, bed shear stress and friction on the foreshore of a microtidal beach. *Coastal Engineering*, 68:6-16.

Raubenheimer, B. Observations and predictions of fluid velocities in the surf and swash zones. Journal *of Geophysical Research*, 107, 3190., doi:10.1029/2001JC001264.

Raubenheimer, B., S. Elgar., & R. T. Guza., 2004. Observations of swash zone velocities: A note on friction coefficients. *Journal of Geophysical Research*, 109, C01027., doi:10.1029/2001JC001264.

Rodi,W., 1993. TurbulenceModels and Their Application in Hydraulics -AState-of-the-Art Review. *Int. Assoc. for Hydryaul. Res.*,

Delft, Netherlands.

Sørensen, O.R., Schaffer, H.A., Sørensen, L.S., 2004. Boussinesq-type modelling using an unstructured finite element technique. *Coastal Engineering*, 50: 181–198.

Torres-Freyermuth, A., Losada, I. J., and Lara, J. L., 2007. Modeling of surf zone processes on a natural beach using Reynolds-Averaged Navier-Stokes equations. *Journal of Geophysical Research*, 112(L05601)., doi: 10.1029/2006JC004050.

Torres-Freyermuth, A., J. L. Lara, and I. J. Losada., 2010. Numerical modelling of short- and long-wave transformation on a barred beach. *Coastal Engineering*, 57(3), 317–330., doi:10.1016/j.coastaleng.2009.10.013.

Torres-Freyermuth, A., Puleo, J. A., & D. Prokrajac., 2013. Modelling swash zone hydrodynamics and shear stresses on planar slopes using Reynolds-Average Navier-Stokes equations. *Journal of Geophysical Ressearch Oceans*,118:1-15., doi:10.1002/jgrc.20074.

Williams, J.; Buscombe, D.; Masselink, G.; Turner, I.L., and Swinkels, C., 2012. Barrier Dynamics Experiment (BARDEX): Aims, design and procedures. *Coastal Engineering*, 63, 3-12.

Zhang, Q., & P. L.-F. Liu.,2008. A numerical study of swash flows generated by bores. *Coastal Engineering*, 55(12), 1113–1134., doi:10.1016/j.coastaleng.2008.04.010.